REPORT DOCUMENTATION PAGE

Form Approved
OMB No. 0704-0188

Public reporting burden for this collection of information is estimated to average 1 hour per response, including the time for reviewing instructions, searching existing data sources, gathering and maintaining the data needed, and completing and reviewing this collection of information. Send comments regarding this burden estimate or any other aspect of this collection of information, including suggestions for reducing this burden to Department of Defense, Washington Headquarters Services, Directorate for Information Operations and Reports (0704-0188), 1215 Jefferson Davis Highway, Suite 1204, Arlington, VA 22202-4302. Respondents should be aware that notwithstanding any other provision of law, no person shall be subject to any penalty for failing to comply with a collection of information if it does not display a currently valid OMB control number. **PLEASE DO NOT RETURN YOUR FORM TO THE ABOVE ADDRESS.**

1. REPORT DATE *(DD-MM-YYYY)*	**2. REPORT TYPE**	**3. DATES COVERED** *(From - To)*
August 2013	Journal Article	August 2013- October 2013

4. TITLE AND SUBTITLE
Thermosetting Poly(imide silsesquioxane)s Featuring Reduced Moisture Affinity and Improved Processability (post-print)

5a. CONTRACT NUMBER
In-House

5b. GRANT NUMBER

5c. PROGRAM ELEMENT NUMBER

6. AUTHOR(S)
Dana M. Pinson, Gregory R. Yandek, Timothy S. Haddad, Elizabeth M. Horstman, Joseph M. Mabry

5d. PROJECT NUMBER

5e. TASK NUMBER

5f. WORK UNIT NUMBER
Q0BG

7. PERFORMING ORGANIZATION NAME(S) AND ADDRESS(ES)

Air Force Research Laboratory (AFMC)
AFRL/RQRP
10 E. Saturn Blvd.
Edwards AFB, CA, 93524-7680

8. PERFORMING ORGANIZATION REPORT NO.

9. SPONSORING / MONITORING AGENCY NAME(S) AND ADDRESS(ES)

Air Force Research Laboratory (AFMC)
AFRL/RQR
5 Pollux Drive.
Edwards AFB, CA, 93524-7048

10. SPONSOR/MONITOR'S ACRONYM(S)

11. SPONSOR/MONITOR'S REPORT NUMBER(S)
AFRL-RQ-ED-JA-2013-216

12. DISTRIBUTION / AVAILABILITY STATEMENT
Approved for public release; distribution unlimited

13. SUPPLEMENTARY NOTES
Journal article published in the ACS Macromolecules Vol. #46, Issue #18 September 2013.
PA Case Number: #13496; Clearance Date: 10 Oct 2013.
© 2013 American Chemical Society
The U.S. Government is joint author of the work and has the right to use, modify, reproduce, release, perform, display, or disclose the work.

14. ABSTRACT
With the goal of improving the moisture resistance of thermosetting polyimides, a thermally stable, polyhedral oligomeric silsesquioxane (POSS) dianiline, which features an aromatic periphery, was co-oligomerized with 4,4′(hexafluoroisopropylidene)diphthalic anhydride (6-FDA), 4,4-diaminodiphenyl ether (ODA), and phenylethynylphthalic anhydride (PEPA) to form thermosetting oligomers of a prescribed number of repeat units. The resultant oligomers were characterized for their chemical architecture, rheological characteristics, and cure behavior. POSS regioisomerism provided a unique opportunity to study the effects of monomer architecture on properties. The type of isomer affects rheological and cure characteristics but was found to have no discernible influence on cured state properties. The benefits of POSS co-oligomerization are 3-fold in that processability, thermal stability, and moisture resistance are each improved. Cured glass transition temperature is reduced, however, for a fixed number of repeat units, due to increased length and molecular weight between cross-links concomitant with POSS co-oligomerization.

15. SUBJECT TERMS

16. SECURITY CLASSIFICATION OF:			**17. LIMITATION OF ABSTRACT**	**18. NUMBER OF PAGES**	**19a. NAME OF RESPONSIBLE PERSON**
					Joseph Mabry
a. REPORT	**b. ABSTRACT**	**c. THIS PAGE**			**19b. TELEPHONE NO** *(include area code)*
Unclassified	**Unclassified**	**Unclassified**	SAR	16	5-5857

Standard Form 298 (Rev. 8-98)
Prescribed by ANSI Std. 239.18

Macromolecules

Article

pubs.acs.org/Macromolecules

Thermosetting Poly(imide silsesquioxane)s Featuring Reduced Moisture Affinity and Improved Processability

Dana M. Pinson,[†] Gregory R. Yandek,*[,‡] Timothy S. Haddad,[†] Elizabeth M. Horstman,[†] and Joseph M. Mabry[‡]

[†]ERC, Inc., Edwards AFB, California 93524, United States

[‡]Air Force Research Laboratory, Rocket Propulsion Division, Edwards AFB, California 93524, United States

ABSTRACT: With the goal of improving the moisture resistance of thermosetting polyimides, a thermally stable, polyhedral oligomeric silsesquioxane (POSS) dianiline, which features an aromatic periphery, was co-oligomerized with 4,4′-(hexafluoroisopropylidene)diphthalic anhydride (6-FDA), 4,4′-diaminodiphenyl ether (ODA), and phenylethynylphthalic anhydride (PEPA) to form thermosetting oligomers of a prescribed number of repeat units. The resultant oligomers were characterized for their chemical architecture, rheological characteristics, and cure behavior. POSS regioisomerism provided a unique opportunity to study the effects of monomer architecture on properties. The type of isomer affects rheological and cure characteristics but was found to have no discernible influence on cured state properties. The benefits of POSS co-oligomerization are 3-fold in that processability, thermal stability, and moisture resistance are each improved. Cured glass transition temperature is reduced, however, for a fixed number of repeat units, due to increased length and molecular weight between cross-links concomitant with POSS co-oligomerization.

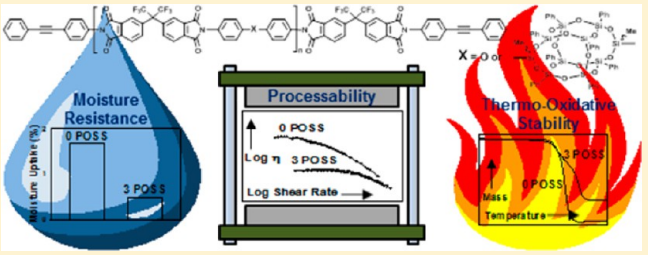

1. INTRODUCTION

Polyimides are commonly utilized by the electronics, automotive, and aerospace industries because of their excellent thermal stability, mechanical properties, and chemical resistance.[1] In aerospace applications, high strength-to-weight ratio organic matrix composites (OMCs) are often fabricated from thermosetting polyimides, which are integrated into the hot sections of aircraft frames and engine components.[2−4] Polyimide chemistry is highly versatile due to the variety of capable monomers used in their syntheses. Therefore, a number of polyimides are commercially available. Their properties are a consequence of their chemical repeat unit architecture, featuring a substantial degree of aromaticity and the ability to form charge transfer complexes (CTC), both intra- and intermolecularly. CTC interactions occur between electron-rich nitrogen atoms (donors) and electron-poor carbonyl groups (acceptors), which are characteristic of the imide group. These interactions can fortuitously act as physical cross-links, which augment creep resistance, tensile properties, and intransigence to thermally induced relaxation.[5,6] However, the electronegativity of the carbonyl groups influences the susceptibility of hydrogen bonding with capable low molecular weight species, most pervasively environmental water.[7] Moisture uptake in polyimides is dependent on the nature of their backbone chemistry and has been measured to be greater than 3% by weight in the saturated state in some cases.[8,9] The consequences of moisture ingress transcend a mere weight penalty; resident water molecules tend to reduce polymer glass transition temperature (T_g) and thermomechanical properties due to plasticization.[10] Furthermore, moisture can precipitate microcrack formation due to associated polymer relaxation processes[11,12] as well as fiber reinforced OMC delamination as a consequence of rapid moisture liberation during heating.[13] Protective approaches against moisture uptake in polyimide-based OMCs include the application of barrier coatings, the inclusion of matrix-phase nanoparticles,[14−16] and the use of constituent monomers that deliver minimal affinity for water in the polymerized state.[17−20] Of these approaches, the latter is most effective because nanoparticles often increase polymer viscosity, impacting processing, while coatings require regular inspection and maintenance. However, the paramount challenge in the pursuit of novel monomer chemistries is maintaining the highest degree of thermal properties expected of polyimides. The insertion of monomers possessing hydrophobic character, such as those possessing aliphatic and fluorinated groups, often reduce T_g and thermal stability. One promising approach is the use of siloxane monomers, which are intrinsically hydrophobic and thermally stable, depending on architecture.[21,22] Recently, Kakimoto et al. reported a hybrid organic−inorganic approach to modifying Kapton-like thermoplastic involving the copolymerization of pyromellitic dianhydride (PMDA) with a POSS diamine oligomer in place of oxidianiline (ODA) to produce a material that exhibited ∼80% less saturated moisture content than its non-POSS counterpart.[23] However, this improvement was realized at

Received: June 27, 2013
Revised: August 5, 2013
Published: September 11, 2013

ACS Publications © 2013 American Chemical Society

the expense of T_g, where the copolymers demonstrated ~100 °C lower T_g than that of PMDA−ODA. We attribute this reduction to the relatively large size of the silsesquioxane monomer used, which imparts lower packing efficiency, reduced propensity for CTC interactions, and a higher overall degree of free volume. Macroscopically, these attributes manifest in lower polymer density and reduced thermally influenced viscoelastic properties.

Despite this shortcoming, there is substantial merit in the application of silsesquioxanes to imide-based thermosetting systems and has been investigated by others.[24,25] In contrast to thermoplastic materials, molecular packing in thermosets is primarily influenced by cross-link density. Therefore, the relatively large size of POSS may influence T_g to a lesser extent. Previously, Wright et al. examined the synthesis, cure kinetics, and thermal properties of arylethynyl-terminated coPOSS imide oligomers, revealing little influence of peripherally cyclopentyl Si_8O_{12} POSS diamine content (up to 10 wt %) on cured T_g.[24] More recently, in collaboration with the Air Force Research Laboratory, Lee investigated the effects of PEPI (phenylethynylphthalimide)-POSS architecture on its cure kinetics and thermal transitions/relaxations.[25] However, no studies to date have investigated moisture uptake in thermosetting POSS-polyimide materials nor sought to understand the effects on viscoelastic properties resulting from POSS co-oligomerization. Therefore, we have chosen one of the recently reported monomeric POSS dianilines[26] to synthesize a new class of thermosetting poly(imide silsesquioxane) copolymers, which were analyzed for their rheological properties, cure kinetics, and delivered properties, including moisture absorption, in the cured state. Our monomer choice also affords a unique opportunity to study the effects of isomeric variations in thermoset monomer constituents as it provides versatile stereochemistry.

2. EXPERIMENTAL DETAILS

Materials. The oligomer framework utilized in this study is derived from 4,4′-(hexafluoroisopropylidene)diphthalic anhydride (6-FDA) and 4,4′-diaminodiphenyl ether (ODA), which were purchased from Lancaster Synthesis Inc., as well as phenylethynylphthalic anhydride (PEPA) serving as the reactive end-cap functionality, which was procured from Maverick Corporation. The 6-FDA, ODA, and PEPA were purified by sublimation under dynamic vacuum. Bis(4-anilinylmethylsilyloxy)octaphenylsilsesquioxane (dianiline POSS, cis and trans) was synthesized using a previously reported method from a POSS tetrasilanol purchased from Hybrid Plastics.[26] Anhydrous 1-methyl-2-pyrolidinone (NMP), methanol (MeOH), and hexanes were acquired from Sigma-Aldrich. HPLC grade chloroform (Burdick and Jackson), HPLC grade toluene (J.T. Baker), and methanol (Fisher Scientific) were all used as received from their respective vendors.

Synthesis. The nomenclature and monomer content for the oligomers synthesized in this study are shown in Table 1. For each oligomer reaction, the 6-FDA monomer was slowly added to an anhydrous NMP solution of POSS and/or ODA in a dry nitrogen environment; the ratio of dianhydride to diamines was 4.0:5.0. After allowing the reaction to proceed for 60 min, an NMP solution of PEPA (2 mol equiv) was then added for a total solute concentration of 20 wt %. The reaction was then stirred overnight under a dry nitrogen blanket. Subsequently, a 1−2 mL aliquot of the amic acid solution was removed for separate analysis. This aliquot was added dropwise to ether and allowed to stir overnight. The solid precipitate was collected by filtration and washed with ether, with the exception of the pure cis-POSS containing oligomers, where hexane was used in place of ether. The solid amic acid oligomer was then dried under vacuum. The remainder of the reaction mixture was diluted with an equivalent volume of toluene and then heated overnight at 155 °C, using Dean−Stark methodology to promote imidization. The reaction was cooled to room temperature, and the product was precipitated into MeOH. The solid product was collected by filtration and washed with methanol. Residual NMP was removed by extraction with water. The final solid product was then dried under vacuum to render powders.

0 POSS. 6-FDA (3.828 g, 8.617 mmol), ODA (2.157 g, 10.772 mmol), and PEPA (1.069 g, 4.306 mmol). Off-white solid (5.89 g, 88% yield). Elemental analysis, found (calculated): C, 64.98 (65.21); H, 2.38 (2.61); F, 14.44 (14.73); N, 4.74 (4.53).

1 cis/trans-POSS. 6-FDA (2.9407 g, 6.620 mmol), ODA (1.3251 g, 6.620 mmol), cis/trans-POSS (2.2106 g, 1.655 mmol), and PEPA (0.8629 g, 3.309). Off-white solid (5.94 g, 85% yield). Elemental analysis, found (calculated): C, 61.40 (61.90); H, 2.82 (3.00); F, 11.74 (10.78); N, 3.48 (3.31).

1 cis-POSS. 6-FDA (0.8402 g, 1.891 mmol), ODA (0.3786 g, 1.891 mmol), cis-POSS (0.6316 g, 0.473 mmol), and PEPA (0.2583 g, 1.040 mmol). Off-white solid (1.37 g, 69% yield). Elemental analysis, found (calculated): C, 60.83 (61.90); H, 2.83 (3.00); F, 11.79 (10.78); N, 3.50 (3.31).

1 trans-POSS. 6-FDA (0.8402 g, 1.891 mmol), ODA (0.3786 g, 1.891 mmol), trans-POSS (0.6316 g, 0.473 mmol), and PEPA (0.2583 g). Off-white solid (1.80 g, 90% yield). Elemental analysis, found (calculated): C, 60.34 (61.90); H, 2.89 (3.00); F, 11.58 (10.78); N, 3.46 (3.31).

3 cis/trans-POSS. 6-FDA (1.3665 g, 3.076 mmol), ODA (0.3082 g, 1.539 mmol), cis/trans-POSS (3.082 g, 2.307 mmol), and PEPA (0.4202 g, 1.693 mmol). Off-white solid (4.05 g, 81.0% yield). Elemental analysis, found (calculated): C, 58.00 (58.74); H, 3.29 (3.38); F, 7.46 (7.01); N, 2.22 (2.15).

3 cis-POSS. 6-FDA (1.3665 g, 3.076 mmol), ODA (0.3082 g, 1.539 mmol), cis-POSS (3.082 g, 2.307 mmol), and PEPA (0.4202 g, 1.693 mmol). Off-white solid (2.35g, 47% yield). Elemental analysis, found (calculated): C, 57.20 (58.74); H, 3.29 (3.38); F, 7.47 (7.01); N, 2.15 (2.15).

3 trans-POSS. 6-FDA (1.3665 g, 3.076 mmol), ODA (0.3082 g, 1.539 mmol), trans-POSS (3.082 g, 2.307 mmol), and PEPA (0.4202 g, 1.693 mmol). Off-white solid (4.40 g, 88% yield). Elemental analysis, found (calculated): C, 57.57 (58.74); H, 3.42 (3.38); F, 7.06 (7.01); N, 2.14 (2.15).

Table 1. Oligomer Nomenclature and Equivalents of Monomers Used in Each of Their Syntheses

compound	PEPA	6-FDA	ODA	POSS
0 POSS	2	4	5	0
1 cis/trans-POSS	2	4	4	1 (cis/trans)
1 cis-POSS	2	4	4	1 (cis)
1 trans-POSS	2	4	4	1 (trans)
3 cis/trans-POSS	2	4	2	3 (cis/trans)
3 cis-POSS	2	4	2	3 (cis)
3 trans-POSS	2	4	2	3 (trans)

Instrumentation and Characterization Details. NMR spectra were collected using Bruker 300 and 400 MHz spectrometers. All spectra were referenced to residual ^1H or ^{13}C in the chosen carrier solvent. ^{29}Si spectra were obtained using an inverse gated 30° pulse sequence with a 12 s delay between pulses and were referenced to external $SiMe_4$ at 0 ppm. GPC data were collected using RI and LS detectors (Wyatt) with a flow rate of 1.0 mL/min for 30 min. Elemental analysis was outsourced to Atlantic Microlab Inc.

Rheological Analysis of Oligomers. The rheological characteristics of the oligomers were measured using an Anton Paar Modular Compact Rheometer MCR 500 coupled with a TC 30 temperature control unit. All measurements were conducted using a 25.4 mm diameter parallel plate at 0.7 mm gap space under a nitrogen blanket at 250 °C. This temperature was chosen as it is above the T_gs of the uncured oligomers and below the cure initiation temperature of the ethynyl group. To prepare the samples for testing, 0.4 g of each oligomer powder was consolidated in a circular mold of equivalent diameter in a Carver laboratory press, at room temperature. Two different experiments were performed. First, oscillatory experiments were conducted at a strain amplitude of 0.1%, within the linear viscoelastic regime of the resins as

dx.doi.org/10.1021/ma401347q | Macromolecules 2013, 46, 7363−7377

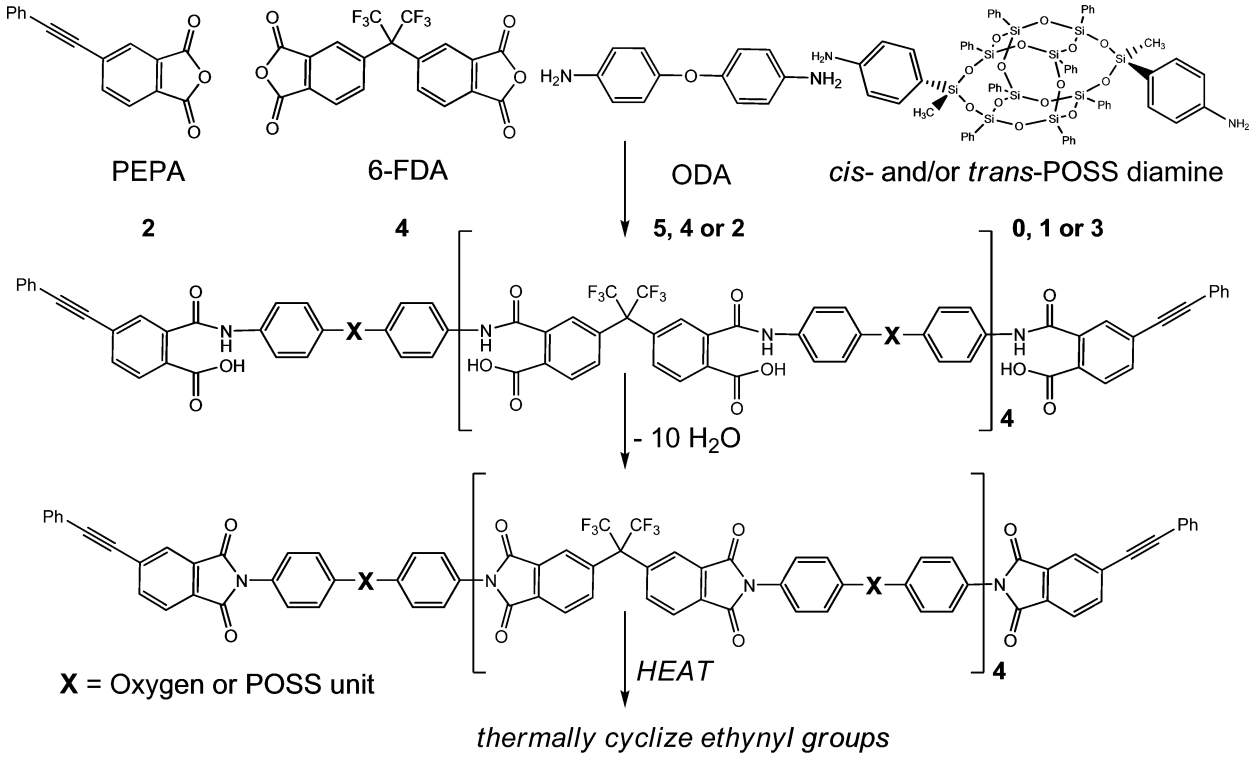

Figure 1. General synthesis scheme of phenylethynyl-terminated POSS-containing oligoimides with an average degree of polymerization of four.

determined from variable amplitude experiments. This experiment was performed to decouple complex moduli in the frequency regime 0.05−500 rad/s. Subsequently, a second set of steady shear experiments were performed in the shear rate regime 10^{-5}−1 s^{-1} to ascertain the shear rate influence on viscosity.

Thermal Analysis. To analyze the cure behavior of the oligomers, differential scanning calorimetry (DSC) was performed using a TA Instruments Q200 coupled with an RCS90 refrigeration cooling system, with a cell nitrogen purge of 50 mL/min. Cure kinetics were analyzed by monitoring the evolution of the T_g after each of six 10 min isothermal increments at the prescribed temperature. Because of the high activation energy of the phenylethynyl group and the number of oligomers investigated, only one sample was utilized for each cure temperature. Although an absolutely precise kinetics evaluation would require the use of a fresh sample for each isothermal exposure, applying 10 min increments to a sample and postcycling to measure the resultant T_g was deemed sufficient for the purposes of this study. Extent of conversion was ascertained by the DiBenedetto method which is presented in detail later, and reaction rate constants and exponents were calculated therefrom after application of a suitable reaction kinetics model.

Thermogravimetric analysis (TGA) was performed using a TA Instruments Q5000 under nitrogen and air atmospheres at a purge rate of 25 mL/min. In general, 5 mg of each sample was tested in a platinum pan, and beyond isothermal steps, a 10 °C min^{-1} ramp rate was implemented. In some cases, a Pfeiffer Vacuum ThermoStar Gas Analysis System was utilized to facilitate mass spectrometry of the gaseous byproducts emanating from the materials during TGA. This system consists of a heated (170 °C) quartz capillary interfaced with the Q5000 chamber, which in turn is connected to the ThermoStar. A vacuum pump pulls the gaseous byproducts through an ionization source, where electron bombardment occurs, followed by ion separation through the quadrupole mass filter, ultimately undergoing analysis by the ion detection system. Bargraph cycle scans were ran for all of the experiments consisting of a repeating detector sweep of m/z in the range of 1−199 atomic mass units (amu). Customized software was used to analyze the bargraph cycle scan data yielding 2-D plots of amu as a function of temperature.

Disk Processing through Thermal Cure of Oligomers. To fabricate cured disks for analysis, 0.4 g of each oligomer was placed in a cylindrical, piston-type steel mold with a 12.7 mm diameter internal cavity in between two pieces of Teflon cut to the shape of the inner cavity. After assembling the mold, it was placed in between the two platens of a laboratory compression molding machine. Volatile removal was facilitated by heating the platens to 300 °C while exerting a pressure of 10 psi with the mold cavity under vacuum. After this step, the pressure was increased to 170 psi and the temperature to 370 °C. This condition was held for 1.5 h to promote phenylethynyl cure. The mold was subsequently cooled and the disk was ultimately extracted.

Density Measurements. To measure the densities of the cured disks, calcium chloride ($CaCl_2$) solutions in deionized water were tuned by varying their salt content until each immersed disk exhibited a suspended state (neither sinking nor rising), thus indicating a density match. Care was taken to ensure that the disks did not have adhered surface air bubbles, which would compromise the measurement. In general, 1.4000 g/cm^3 solutions (~38% $CaCl_2$) were used as a starting point. Each disk was immersed in the solution, and deionized water was added dropwise followed by stirring until the required condition was observed. The amount of deionized water added during this process was used to calculate the density of final solution.

Relative Humidity Exposure. Moisture diffusion experiments on the cured disks were conducted in a Tenney ETCU09RC-5.0-F environmental test chamber set at 80% relative humidity and 80 °C. In this system, humidity is supplied to the chamber via vaporized deionized water. The disks were situated on a custom platform such that both sides of each disk were exposed to the local environment. At incrementing times, the disks were removed from the chamber, and any surface moisture was gently removed using a gaseous nitrogen purge stream. The disks were then weighed using a Sartorius LA 230 S balance situated on a granite slab. The experiments were conducted for 1000 h, with a higher frequency of weight measurements conducted during the first day of exposure. The data were analyzed to determine saturated moisture uptake as well as fitting the experimental data using Fick's second law of diffusion to calculate diffusion coefficients.

Thermomechanical Analysis (TMA). To ascertain the effects of resident water on the viscoelastic properties of the cured specimens,

dx.doi.org/10.1021/ma401347q | *Macromolecules* 2013, 46, 7363−7377

Table 2. Theoretical MW and Experimental MW Determined from SEC and Elemental Analysis (Extrapolated from Determined Atom Content) for All Oligomers

oligomer	theor MW	M_n[a]	M_w[a]	theor no. of C atoms per chain	MW[b] (C)	theor no. of H atoms per chain	MW[b] (H)	theor no. of N atoms per chain	MW[b] (N)
0 POSS	3094	3700	5200	168	3100	80	3400	10	3000
1 cis/trans-POSS	4230	4100	4700	218	4300	126	4500	10	4000
1 cis-POSS	4230	4500	5600	218	4300	126	4500	10	4000
1 trans POSS	4230	4900	5100	218	4300	126	4400	10	4100
3 cis/trans-POSS	6501	5900	6200	318	6600	218	6700	10	6300
3 cis-POSS	6501	6200	6300	318	6700	218	6700	10	6500
3 trans-POSS	6501	7100	14000	318	6600	218	6400	10	6500

[a]MW Determined from SEC. [b]MW determined from elemental analysis.

Table 3. ^{1}H NMR Integral Values for the Oligoimides Investigated in This Study

	0.0−1.5 ppm		7.0−7.7 ppm		7.7−8.5 ppm	
oligomer	expected	observed	expected	observed	expected	normalized to
0 POSS	0	0	50	57.1	30	30
1 cis/trans-POSS	6	6.3	86	78.1	34	34
1 cis-POSS	6	4.5	86	77.6	34	34
1 trans-POSS	6	5.0	86	78.5	34	34
3 cis/trans-POSS	18	20.6	158	183.4	42	42
3 cis-POSS	18	24	158	186.1	42	42
3 trans-POSS	18	19.4	158	152.7	42	42

dynamic TMA experiments were performed with a TA Instruments Q400. Both dry samples and moisture-saturated samples were tested under identical conditions for the purposes of comparison. A high heating rate was employed (50 °C min^{-1}) to minimize moisture release during each scan. A static expansion probe force of 0.1 N was applied to each sample with a force modulation of 0.1 N at a frequency of 1.0 Hz. All samples were rapidly heated to 400 °C, and data were recorded at 1 point/s. The onset point corresponding to the drop in storage modulus was used as the point of comparison between the dry and wet samples.

3. RESULTS AND DISCUSSION

The synthesis of the POSS containing oligomers, as well as the 0 POSS (control) material, generally involved the reaction of 6-FDA dianhydride with the POSS dianiline and/or ODA, end-capped with PEPA, as depicted in Figure 1. The targeted reaction products were AB oligomers with an *average* chain length of 5 diamines and 4 dianhydrides, end-capped with monofunctional anhydrides. Each chain is expected to have two thermally reactive ethynyl groups, which can cyclize to form a cross-linked network. The first stage of the reaction involves formation of oligoamic acids by the slow addition of 6-FDA dianhydride to an anhydrous NMP solution of diamines, followed by encapping with monofunctional PEPA. The diamines, either ODA or a mixture of ODA and POSS diamines, are always present in excess, thus preventing high molecular weight materials from forming. In addition, the POSS dianilines are produced in three isomers: pure *cis*-, pure *trans*-, and a 50:50 mixture of *cis*- and *trans*-dianilines. Each unique set of POSS monomers was used to synthesize one of three respective oligomer types. Following a Dean−Stark protocol to remove water, the oligoamic acids were converted to oligoimides with no POSS, 1 POSS unit per chain, and 3 POSS units per chain. These materials were isolated by precipitation into methanol and dried under dynamic vacuum to yield off-white powders in good yield. These soluble oligoimides were fully characterized by elemental analysis, GPC, and NMR spectroscopy to determine composition and molecular weight.

Elemental analysis and GPC data (Table 2) were used in conjunction with proton NMR integration data (Table 3) to confirm that the approximate target chain lengths were achieved. Combustion elemental analysis data were collected in duplicate and are presented as an average. Oligomer molecular weight was calculated from the structure shown in Figure 1. In general, the molecular weight obtained from the % C present matches within 2−3% of the theoretical value. The molecular weight from % H tends to be high, while % N gives values lower than expected. While this analysis method is by no means quantitative, it does indicate that the oligomers do have an average degree of AB copolymerization of approximately four and are end-capped with two phenylethynyl groups. This is corroborated by the oligomer GPC data (Table 2) which indicate molecular weights in the expected range.

In ^{1}H NMR spectra (Figure 2), the peaks from 7.7 to 8.5 ppm are attributed to 6-FDA and the three protons of a similar environment on the phenyl ring of PEPA. The integral in this region increases by four protons with each additional POSS per

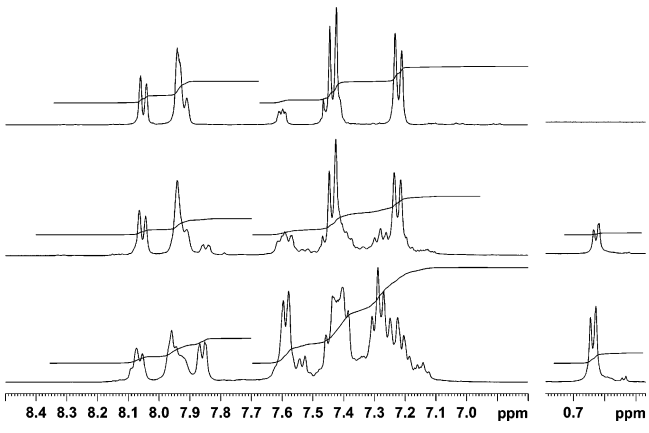

Figure 2. ^{1}H NMR of oligoimides in CD_2Cl_2: upper trace, 0 POSS; middle trace, 1 cis/trans-POSS; lower trace, 3 cis/trans-POSS. These spectra delineate the regions integrated to corroborate molecular weight (see text).

dx.doi.org/10.1021/ma401347q | *Macromolecules* 2013, 46, 7363−7377

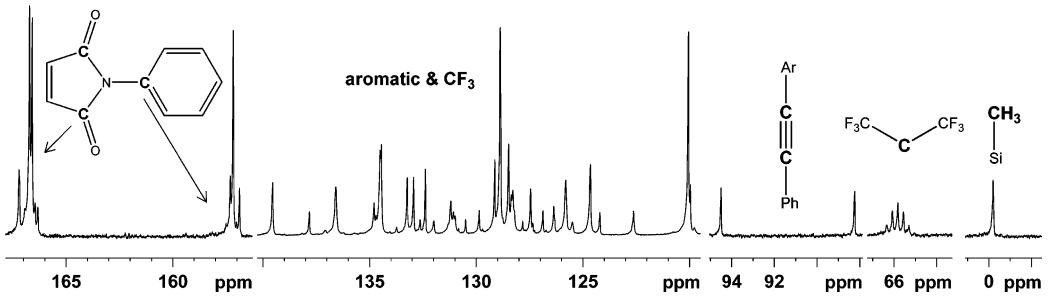

Figure 3. Representative ^{13}C NMR of 1 cis/trans-POSS oligoimide in CD_2Cl_2. Functional group assignments are shown; the section from 140 to 120 ppm is displayed at 1/4 the intensity of the other four regions.

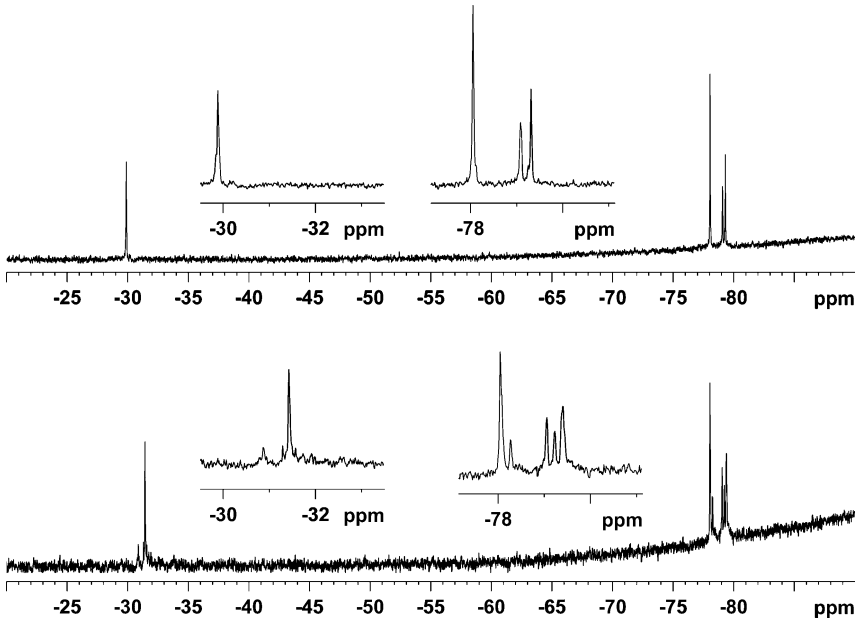

Figure 4. ^{29}Si NMR of 3 cis-POSS oligoamic acid in DMSO-d_6 (upper trace) and ^{29}Si NMR of 3 cis-POSS oligoimide in $CDCl_3$ (lower trace).

chain added. This is due to a shielding effect of the electron-withdrawing POSS cage compared to an oxygen atom of ODA on the protons of the POSS aniline group. Consequently, this region was normalized to 30 protons for the 0 POSS oligomer, 34 for the 1 POSS containing oligomers, and 42 for the 3 POSS containing oligomers. The peaks between 6.8 and 7.7 ppm are attributed to the 8 protons of each ODA, the 40 protons from the phenyl rings of each POSS along with the remaining 4 of the aniline POSS protons, and 5 of the aromatic protons in each PEPA. The integrals are shown to increase by the expected amount of 36 protons with each addition and reduction of POSS and ODA, respectively. The peaks between 0.00 and 1.5 ppm are attributed to the two methyl groups of the POSS and increase by 6 with each additional POSS (Figure 2 and Table 3). Once again, the values from the integrated ^1H NMR spectra corroborate what is expected for oligoimides made with the structure shown in Figure 1.

A representative ^{13}C NMR spectrum of the 1 cis/trans-POSS oligoimide, with functional groups assigned to the appropriate regions, is shown in Figure 3. In the carbonyl region (~167 ppm), two sets of peaks are attributed to the carbonyl groups of the 6-FDA and the carbonyl groups of the PEPA end-caps. The two peaks between 88 and 95 ppm are attributed to the acetylene carbons of the PEPA groups, indicating the chains are end-capped. It is not standard practice to integrate ^{13}C NMR spectra because nuclear Overhauser effects (NOE) tend to skew the intensity of the observed signals. Nevertheless, an integration ratio of the aforementioned carbonyl region with the acetylene region (both types of carbon should have minimal if any NOE effect as they are both quaternary carbons) yielded values of approximately 5:1, which is theoretically present in an oligoimide with the structure shown in Figure 1 (an average of 20 carbonyl groups to 4 acetylene carbons in each chain).

In Figure 4, the ^{29}Si NMR spectra of the 3 cis-POSS oligoamic acid and oligoimide are shown. The sharp peaks present in all spectra, along with the absence of peaks in the −40 to −60 ppm range, indicate the POSS cages are intact and are not decomposed by the reaction conditions employed to produce the oligoamic acid or to generate the oligoimide. The increase in the number of spectral lines on conversion from oligoamic acid to oligoimide is attributed to a lower degree of rotational freedom and thus more chemical environments.

Rheology. Figure 5 reveals the dependence of oligoimide viscosity on steady shear rate at 250 °C, well above their measured precure T_gs but below the ethynyl curing temperature. In general, POSS co-oligomerization reduces zero shear viscosity (η_0), extropolated to 10^{-5} s^{-1}, for the majority of the oligomers, by an order of magnitude in comparison with that of 0 POSS. As SEC revealed little deviation from the target molecular weights, viscosity reductions are realized despite increases in oligomer molecular weight ancillary to POSS copolymerization, resulting from the size of POSS interfering with oligomer chain packing

dx.doi.org/10.1021/ma401347q | Macromolecules 2013, 46, 7363−7377

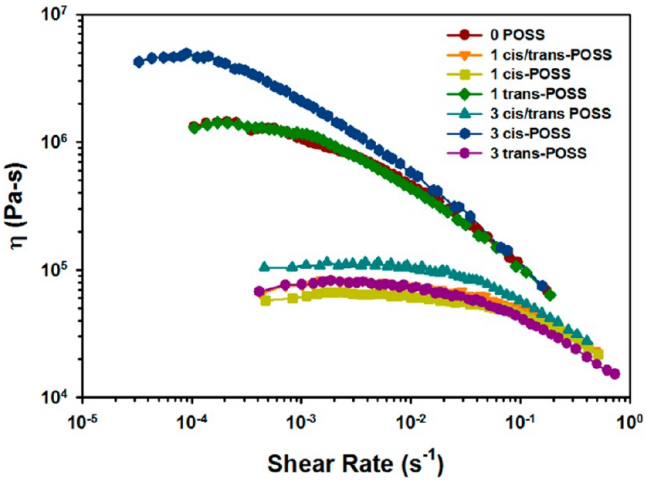

Figure 5. Steady shear viscosity dependence on shear rate for the uncured oligomides at 250 °C.

and CTC interactions. There are, however, two exceptions to this trend. The 1 trans-POSS oligomer demonstrates equivalent behavior to 0 POSS, and the 3 cis-POSS oligomer exhibits significantly higher η_0. This outlying behavior suggests that POSS isomer type affects oligomer packing and orientation and thus response to shear stress.

The rheological response to variable small deformation frequency, again at 250 °C, further illuminates POSS isomer effects. Complex viscosity is decoupled into storage and loss moduli for the three sets of oligomers: (a) cis/trans-, (b) cis-, and (c) trans- in Figure 6. The crossover frequency (indicated by ω_{co}), defined as the equivalency condition of the storage and loss moduli for each respective oligomer, shows dependence on POSS concentration but more significantly isomer type. All oligomers exhibit liquid-like behavior at low frequency as expected. For the cis/trans mixed isomers, the transition to solid-like behavior shifts to higher frequency for both 1 and 3 POSS. ω_{co} for the 1 cis/trans-POSS oligomer occurs at higher frequency than that of 3 POSS, likely due to the higher molecular weight of the latter. For the cis-POSS oligomers, the 1 POSS oligomer again exhibits a ω_{co} at a higher frequency than 0 POSS, but surprisingly, the 3 POSS oligomer demonstrates solid-like behavior near the inception of the freqeuncy sweep. The trans-POSS oligomers, in contrast, demonstrate minimal shift in ω_{co} relative to 0 POSS, largely insensitive to POSS content.

The dependence of the transition from liquid- to solid-like behavior on POSS type could be explained by oligomer geometrical conformation influenced by isomer type and its resultant ability to pack, thus affecting its free volume distribution. The trans-POSS isomer exerts minimal effects on the complex moduli, especially at the lowest investigated POSS concentration, as this isomer type renders more linear chains. In contrast, the cis-POSS isomer, when copolymerized, induces curvature that increases with concentration. Therefore, it is plausible that the 3 cis-POSS material contains oligomers that possess near cyclic conformations, which may interact through some degree of reticulation. This conformational state could impart solid-like behavior in response to shear stress. We found no spectroscopic evidence that chemical reactions are the cause of the unusual solid-like behavior of the 3 cis-POSS oligomer, nor did T_g, solubility in solvents, or processing characteristics change after exposure to 250 °C for 1 h. Lastly, the oligomers possessing a more random distribution of cis- and trans-POSS isomers could

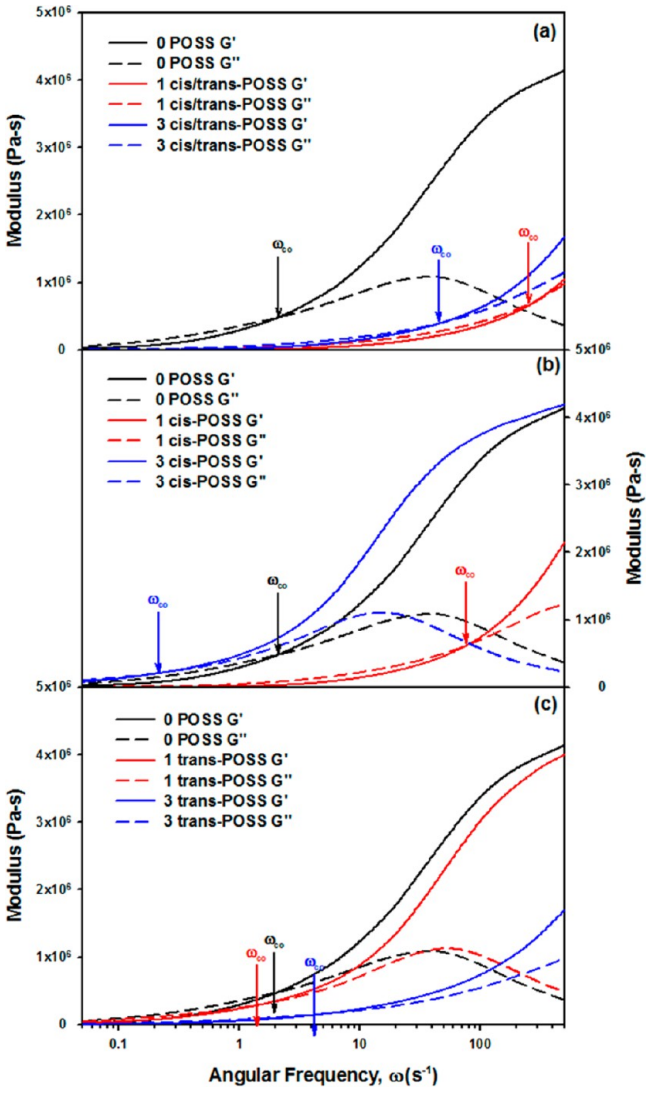

Figure 6. Storage and loss moduli measured from variable frequency oscillatory rheometry experiments at 250 °C for (a) cis/trans-, (b) cis-, and (c) trans-oligomers, in comparison with those of 0 POSS. The crossover frequencies are indicated by ω_{co}.

have the lowest degree of order and interactions; thus, a higher degree of chain conformations could be adopted during oscillatory strain, causing the transition to solid-like behavior to consistently appear at higher frequency. This concept is further illustrated by Figure 7, where the frequency dependence of tan delta (δ) is plotted. Of particular interest, the magnitudes of δ are quite high at low frequencies for the oligomers containing any degree of the cis-POSS isomer, with the exception again of the oligomer containing 3 cis-POSS segments. This data indicates that energy loss is dominant at low frequency in these isomers likely due to the higher degree of free volume present in the oligomer chain ensemble.

Cure Characterization. Isothermal cure kinetics were examined by DSC at five temperatures spanning 300−380 °C. For each cure temperature, the material was held isothermally for 10 min increments, and after each exposure, T_g was measured by cooling the sample to ambient and subsequently sweeping back up to the prescribed temperature at 10 °C min^{-1}. This method is generally effective for evaluating polyimide cure because evolving T_g does not typically exceed cure temperature. The DiBenedetto

dx.doi.org/10.1021/ma401347q | Macromolecules 2013, 46, 7363−7377

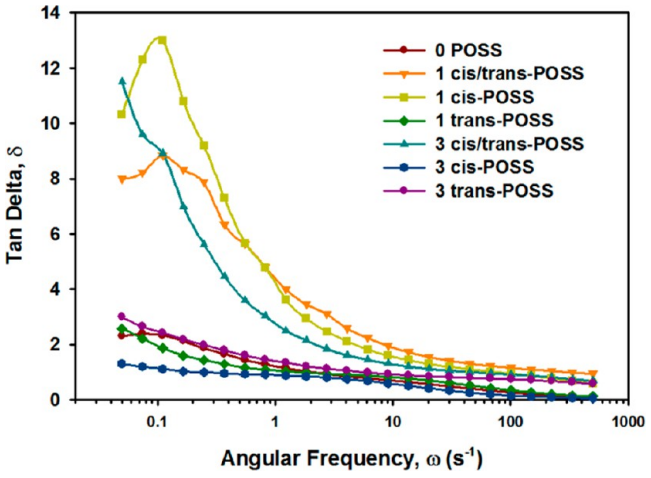

Figure 7. Plots of tan delta as a function of oscillatory frequency for the oligoimides at 250 °C.

equation,[27,28] which has been successfully applied to polyimide thermoset cure by others,[24,29−31] provides a relation between reaction conversion α and measured T_g:

$$\frac{T_g - T_{g,u}}{T_{g,c} - T_{g,u}} = \frac{\lambda\alpha}{1 - (1 - \lambda)\alpha} \quad (1)$$

In this equation, $T_{g,u}$ is that of the uncured oligomer, $T_{g,c}$ is that of the fully cured polymer (assumed to be those measured after 400 °C exposure for 1 h), and λ is the ratio of heat capacities of the cured polymer to uncured oligomer (0.69 was assumed as experimentally determined by Scola et al.[29]) In Figure 8,

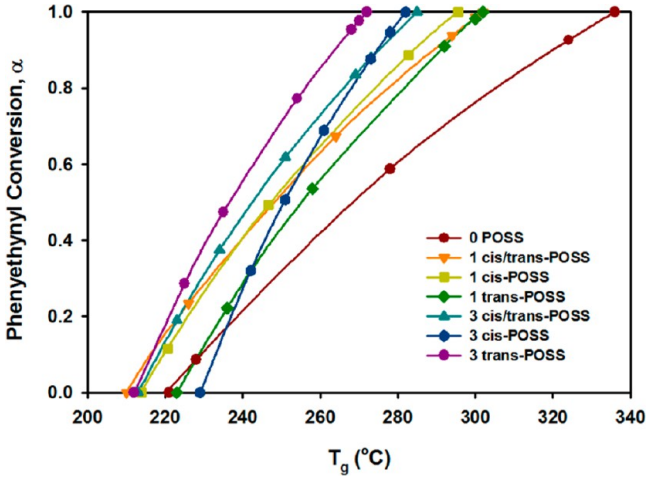

Figure 8. Phenylethynyl conversion, α, calculated from the DiBenedetto equation, plotted as a function of measured T_g for each of the oligoimides.

phenylethynyl conversion, calculated from (1), is plotted against measured T_g for each oligoimide. Prior to cure, oligomer T_gs adhere to their steady shear viscosity characteristics in that the oligomers featuring higher η_0 also demonstrate higher T_g. At a fixed number of repeat units (4), POSS oligomerization reduces fully cured T_g. Isomer type does not exert a clear effect on T_g at full conversion; however, the T_gs appear in groups segregated by POSS concentration. The 3 POSS polyimides exhibit lower T_gs than those of the 1 POSS polymers, which are all lower than that of 0 POSS. This behavior is attributed to lower density due to the higher molecular weight between cross-links concomitant with POSS oligomerization and perhaps to a lesser extent affected by a thermal relaxation within the POSS cage because it is not an absolutely rigid polyhedron.

A first-order reaction rate kinetics model was initially assumed to describe isothermal phenylethynyl cure, as has been successfully applied to other oligoimides with equivalent reactive functionality.[29−33] This rate law was found to accurately model the kinetics of the 0 POSS, 1 cis/trans-, and 1 cis-POSS oligomers but failed to capture the cure behavior of the other oligomer types. To illustrate this disparity in effectiveness, plots of $\ln(1 - \alpha)$ vs reaction time at each isothermal temperature are shown in Figure 9 for 0 POSS and 1 trans-POSS. Predominately,

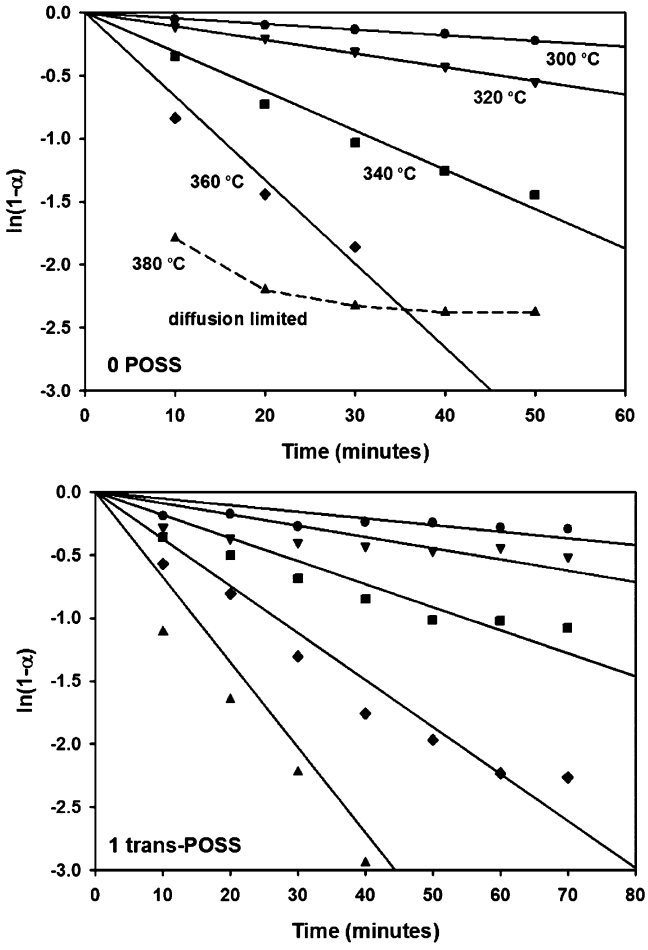

Figure 9. First-order reaction rate analyses of the isothermal conversion data pertaining to the 0 POSS and 1-trans POSS oligoimides. Data points are represented with symbols, and the solid lines are the attempted linear fits. First-order kinetics fails to sufficiently model isothermal cure of 1 trans-POSS.

first-order kinetics (solid lines) provide an excellent fit to the 0 POSS data (symbols) but were found to fail above $\alpha = 0.8$. This is likely due to diffusion governed reactions dominating at high conversion as a consequence of reduced end-group mobility concomitant with network gelation.[29,34] After the first 10 min isotherm at 380 °C, the 0 POSS and 1 POSS oligomers exceed a conversion of 0.8; thus, this temperature was dismissed from first-order fitting. In contrast, the first-order kinetics model does not provide reasonable fits to the experimental data for the 1 trans-POSS, especially at the lower cure temperatures, where R^2

dx.doi.org/10.1021/ma401347q | Macromolecules 2013, 46, 7363−7377

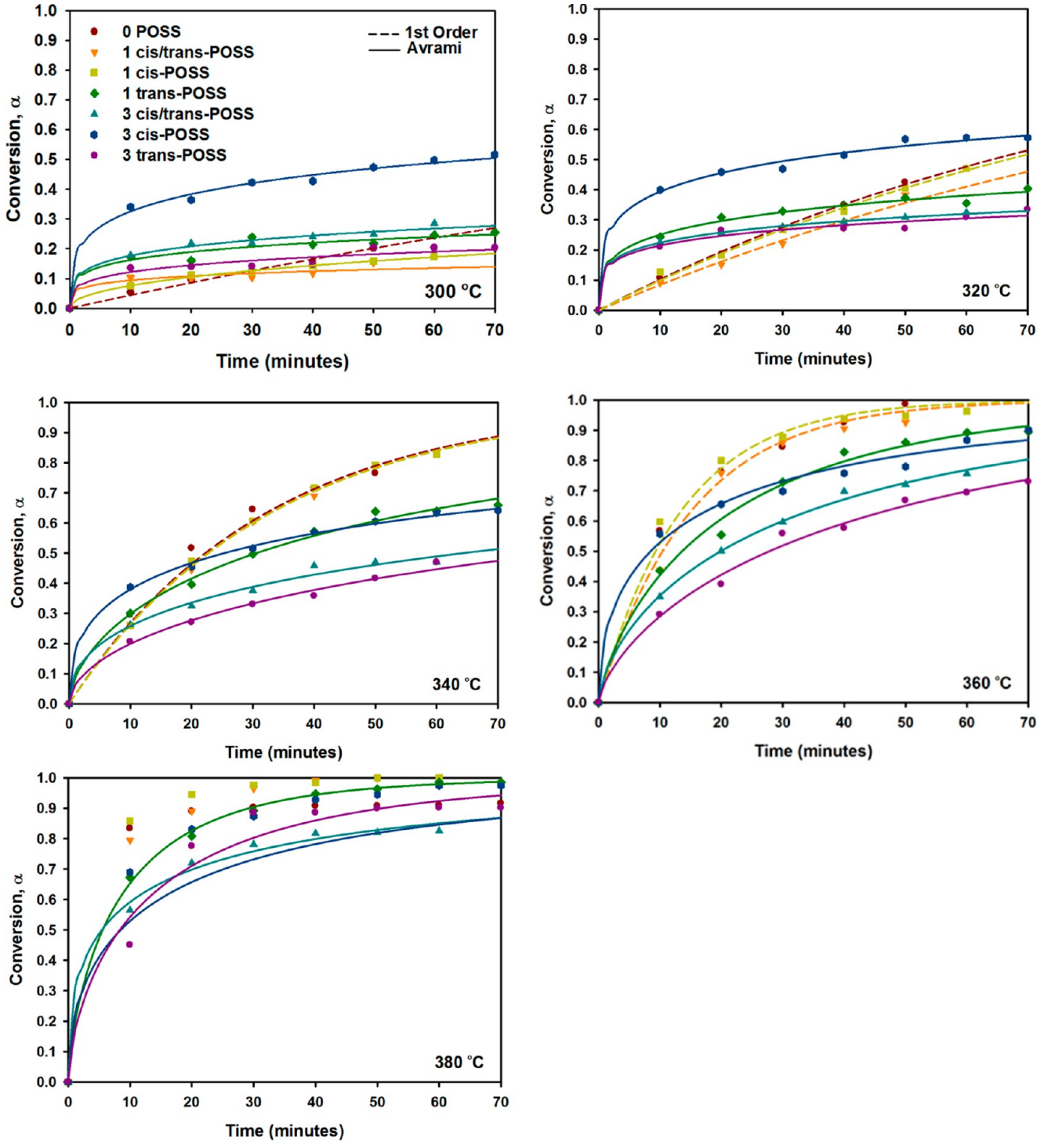

Figure 10. Experimental isothermal conversion vs time data (symbols) and first-order (dashed curves) and Avrami (solid curves) fits (where applicable) for each investigated temperature.

values of 0.49 (300°) and 0.28 (320 °C) were determined. Therefore, attempts were made to fit the remaining data to *n*th-order reaction kinetics, but no values of *n* provided a reasonable fit.

Avrami theory, commonly used to describe liquid−solid transitions in matter, especially those intrinsic to polymer crystallization and nucleation/growth processes, was attempted to fit the unusual reaction kinetics of the 1 trans-, 3 cis/trans-, 3 cis-, and 3 trans-POSS oligoimides. This method has been successfully applied to describe epoxy cure in other works[35,36] but, to our knowledge, has not been used to model phenylethynyl cure. According to this theory, the relationship between conversion, α, and time, t, is described as

$$\alpha = 1 - \exp[-kt^n] \quad (2)$$

where k is the temperature-dependent reaction rate constant and n is the reaction exponent. The integral solution to the first-order rate law is in fact a special case of (2) with $n = 1$. Using the natural log expression of (2), n and k are readily determined from the

dx.doi.org/10.1021/ma401347q | *Macromolecules* 2013, 46, 7363−7377

Table 4. Reaction Exponents and Rate Constants with Associated Coefficients of Determination (R^2) Resulting from Fitting Isothermal Conversion Data to First-Order Reaction Rate and Avrami Conversion Models (k in min^{-n})

	300 °C			320 °C			340 °C			360 °C			380 °C		
oligomer	n	k	R^2	n	k	R^2	n	k	R^2	n	k	R^2	n	k	R^2
0 POSS	1	0.005	0.99	1	0.011	1.00	1	0.031	0.98	1	0.066	0.97			
1 cis/trans-POSS	0.22	0.060	0.56	1	0.009	0.98	1	0.031	1.00	1	0.066	0.99			
1 cis-POSS	0.49	0.026	0.80	1	0.010	1.00	1	0.031	1.00	1	0.075	0.98			
1 trans-POSS	0.25	0.101	0.70	0.28	0.151	0.95	0.60	0.088	0.98	0.77	0.092	0.98	0.73	0.200	0.99
3 cis/trans-POSS	0.26	0.106	0.92	0.23	0.148	1.00	0.45	0.091	0.99	0.68	0.091	0.99	0.42	0.340	0.94
3 cis-POSS	0.30	0.198	0.95	0.28	0.261	0.95	0.40	0.189	0.99	0.51	0.234	0.93	0.60	0.287	0.99
3 trans-POSS	0.27	0.070	0.70	0.23	0.143	0.85	0.55	0.063	0.98	0.71	0.065	0.98	0.67	0.169	0.83

slope and intercept of the line, respectively, in analogous fashion to first-order kinetics:

$$\ln[-\ln(1-\alpha)] = n \ln t + \ln k \quad (3)$$

Overall, the increased flexibility of the two-parameter Avrami equation provides good fits to the remaining data. The experimental data (symbols), the first-order fits (dashed curves), and Avrami fits (solid curves) to that data are shown for each temperature in Figure 10. As discussed earlier, the first-order rate law provides the best fit to the 0 POSS data for all investigated temperatures (see R^2 values in the first row of Table 4). The reaction rate constant expectedly increases with temperature for 0 POSS. The first-order reaction rate kinetics model also provides excellent fits to the 1 cis/trans- and 1 cis-POSS data, with the exception of at 300 °C, where the Avrami equation was found to be more effective. Overall, the 0 and 1 POSS oligomers cure similarly, but the 3 POSS oligomers are contrastive. The 3 POSS oligomers interestingly cure the most rapidly at 300 and 320 °C among all of the oligomers, and for a short time at 340 °C, but this effect vanishes at higher temperatures. This finding suggests that increased free volume imparted by the presence of POSS accelerates the early stages of phenylethynyl cure at the lower investigated temperatures, perhaps via increased oligomer chain diffusion. 3 cis-POSS distinctively cures most rapidly among the 3 POSS family of oligomers. Between 340 and 360 °C, in contrast, the asymptotic conversions of the 3 POSS oligomers are lower than those of the others. Even at 380 °C, after an hour of cure time, full conversion is not achieved, thus requiring additional thermal energy. The phenylethynyl reactions for the 3 POSS oligomers also exhibit less sensitivity to cure temperature. Because the molar mass of the POSS unit is relatively high, its use conceivably requires the input of higher thermal energy to overcome the associated increased mobility and diffusion barrier after a threshold conversion.

To quantify the activation energies (E_a) associated with the phenylethynyl reactions of each of the oligomers, an Arrhenius relationship between the reaction constants and temperature was assumed. The slope of the regression line plotted from the natural log expression of the standard Arrhenius equation was used to calculate E_a. The results of this analysis are shown in Table 5. 0 POSS exhibits an E_a of 33 kcal mol^{-1}, consistent with those found by others for the phenylethynyl reaction of oligomers containing various monomers.[24,25,29,30] The E_as of the 1 cis/trans- and 1 cis-POSS oligomers, excluding their rate constants at 300 °C which did not fit first-order kinetics, are 38 and 37 kcal mol^{-1}, respectively, higher than that of 0 POSS. The E_as of the remaining oligomers were more difficult to calculate due to their complexity. Referring again to Table 4, the 1 trans-, 3 cis/trans-, 3 cis-, and 3 trans-POSS oligomers are described by n ranging from 0.2 to 0.3 between 300 and 320 °C, increasing to 0.4−0.8 in the higher temperature regime. Physical interpretation of this phenomenon in the context of Avrami theory suggests that the change in the growth exponent, precipitated by increasing temperature, indicates a change in the liquid−solid transition mechanism, which is likely in this case to be transcension of the energy barrier for sufficient POSS segment mobility. Examination of the curve fits in Figure 10 reveals that this increase in n is due to the difference in sensitivity of α on time after the first 10 min of cure; at the lower cure temperatures, α increases only slightly after the first 10 min segment, but at the higher cure temperatures, α develops more gradually with cure time. To calculate E_a for the oligoimides described by Avrami theory, the following modified version of the Arrhenius relationship was implemented, consistent with the Avrami equation:

Table 5. Calculated Arrhenius Parameters Pertaining to the Thermal Cure of the Oligoimides Synthesized in This Study

oligomer	$E_{a,1}$	R^2	$E_{a,2}$	R^2
0 POSS	33	1.00		
1 cis/trans-POSS	38	0.99		
1 cis-POSS	37	1.00		
1 trans-POSS	93	1.00	36	1.00
3 cis/trans-POSS	62	0.81	48	0.99
3 cis-POSS	23	1.00	41	0.99
3 trans-POSS	83	0.93	47	1.00

$$k^{1/n} = A e^{-E_a/RT} \quad (4)$$

The natural log expression of (4) also renders the ability to calculate E_a from the slope of the line $(1/n)\ln(k)$ vs $1/T$. Distinguishing the two n regimes for the four oligoimides analyzed by Avrami theory, these lines are plotted in Figure 11, where the blue regression lines are derived from the lower temperature n and k values, while those of the red pertain to the higher temperature reaction parameters. Thus, two E_as for each oligomer are determined, $E_{a,1}$ (blue) and $E_{a,2}$ (red), the values of which are listed in Table 5. The $E_{a,1}$ values for these four oligomers are significantly higher than the E_as of the 0 and 1 POSS oligomers, with the exception of 3 cis-POSS. $E_{a,2}$ for 1 trans-POSS is similar to its other 1 POSS counterparts, and the remaining $E_{a,2}$s are higher than the E_as of the other oligomers.

Moisture Diffusion and Its Effects on T_g. The saturated moisture levels of the cured oligomers in the form of 12.7 mm diameter, ~2 mm thick disks, after 1000 h of exposure to 80 °C/80% relative humidity, are shown in Figure 12a. 0 POSS absorbs 1.7% of its original weight in water, similar to what has been published (~2.3%) on moisture diffusion in thin 6-FDA-ODA thermoplastic polyimide films.[34] This difference is expected because thermosets generally absorb less moisture than thermo-

dx.doi.org/10.1021/ma401347q | Macromolecules 2013, 46, 7363−7377

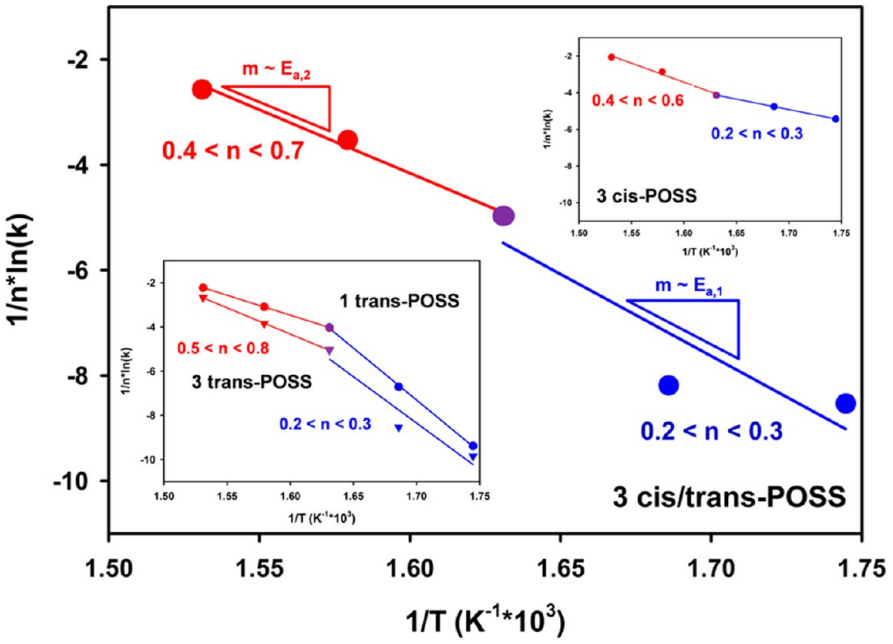

Figure 11. Arrhenius analysis of the cure reactions of the 1 and 3 trans- (lower left inset), 3 cis/trans-, and 3 cis-POSS (upper right inset) oligoimides, highlighting two reaction exponent (n) regimes driven by cure temperature. The purple data points are shared by the two regimes, and m represents the slopes of the regressions, which are equivalent to the activation energies.

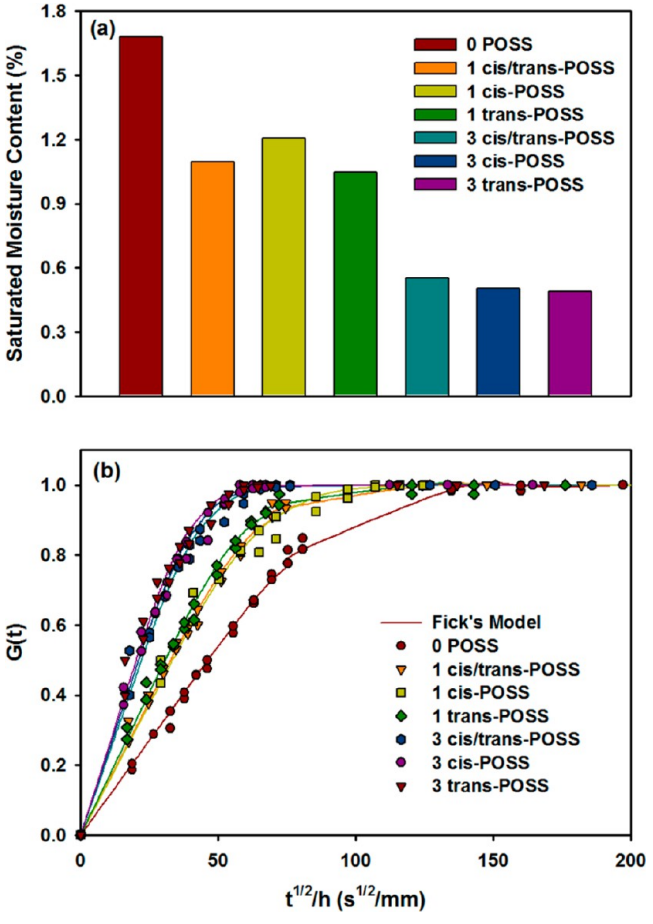

Figure 12. (a) Saturated moisture content of the cured oligoimides after exposure to 80 °C/80 RH for 1000 h and (b) normalized sorption data (symbols) and fits using the Fickian diffusion model (lines).

plastic analogues as the latter have the tendency for increased long time relaxation to accommodate a greater amount of water molecules. Co-oligomerization with POSS decreases saturated moisture content. The 1 POSS polymers take up 28−38% less moisture than 0 POSS, while the 3 POSS materials demonstrate even greater moisture resistance (67−70% less saturated water). No trend is apparent in terms of POSS isomer type.

Normalized experimental moisture ingress data as a function of time for all of the materials are shown in Figure 12b (symbols). The results of data fitting using the Fickian diffusion model are also shown (solid lines). The model used is described by the equation[34]

$$G(t) = \frac{W(t) - W_0}{W_\infty - W_0} = 1 - \frac{8}{\pi^2}\sum_{m=0}^{5}\frac{1}{(2m+1)^2} \times \exp\left[\frac{-D(2m+1)^2\pi^2 t}{h^2}\right] \quad (5)$$

where $W(t)$ is the sample weight at time t, W_0 is the initial sample weight, W_∞ is the weight of the sample in the saturated state, D is the diffusion coefficient, and h is the thickness of the sample. Diffusion coefficients were calculated applying a least-squares minimization of (5), the results of which are shown in Table 6.

Table 6. Disk Thicknesses, Cured Polyimide Densities, and Water Diffusion Coefficients of the Studied Materials

cured oligomer	density (g/cm^3)	thickness, h (mm)	D (mm^2/s × 10^5)
0 POSS	1.360	2.057	2.30
1 cis/trans-POSS	1.343	2.229	4.60
1 cis-POSS	1.367	1.334	4.40
1 trans-POSS	1.342	2.303	5.20
3 cis/trans-POSS	1.314	2.183	10.00
3 cis-POSS	1.309	2.467	10.00
3 trans-POSS	1.310	2.407	12.00

dx.doi.org/10.1021/ma401347q | Macromolecules 2013, 46, 7363−7377

Excellent fits from the application of the Fickian diffusion model are obtained. Examining the data, it is immediately apparent that $G(t)$ appears in three distinct bands, pertaining to the cured 0 POSS, 1 POSS, and 3 POSS polyimides. Not much separation is revealed within the 1 and 3 POSS sets of data, suggesting that POSS isomer type has little effect on the kinetics of water diffusion. The diffusion coefficients increase with POSS content. Coincidentally, the densities of the cured polyimides also decrease with increasing POSS content, as expected, because the cross-link densities should decrease due to the higher molecular weight between cross-links. This finding elucidates greater free volume content introduced by POSS co-oligomerization. Therefore, water molecules have a greater ability to flux due to that free volume. However, although the diffusion rate increases with POSS content, saturated moisture content significantly decreases, suggesting that fewer sites are available for water molecule occupation. This is likely due to the POSS units either shielding the imide carbonyl groups from hydrogen bonding with water, or POSS periphery phenyl groups hydrogen bonding with carbonyl groups from adjacent oligomer segments, or a combination of both factors.

To investigate the effects of reduced saturated water content imparted by POSS co-oligomerization, the wet glass transition temperatures of the polyimides were investigated by TMA. To limit water release from the cured polymers during the scans prior to T_g, a rapid heating rate was employed (50 °C min^{-1}). This rate invariably extended T_g observation to higher temperatures, but the magnitudes are of less importance than the difference between dried and saturated states (the same sample was used for each polymer). T_g was measured by the onset point of the dropoff in storage modulus. The 0 POSS material exhibits a 51 °C decrease in T_g in the saturated state, while the decrease in the 1 cis/trans-POSS is 29 °C and that of the 3 cis/trans-POSS is remarkably 1 °C, as shown in Figure 13. The T_g of the 3 cis/trans-

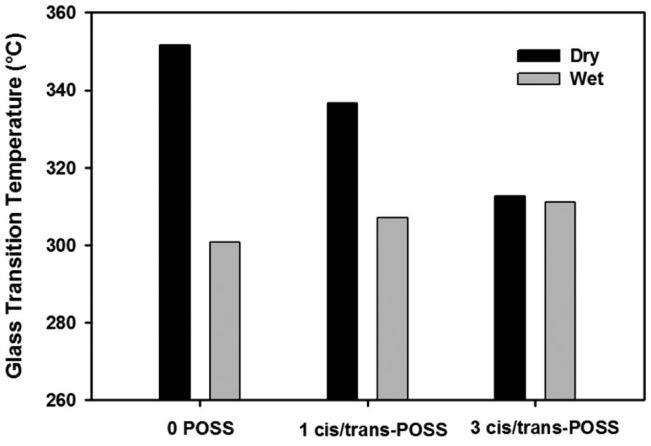

Figure 13. Bar graphs representing the dry and wet T_gs of the cured polyimides measured by rapid scan TMA.

POSS polymer is 10 °C higher than that of 0 POSS in the saturated state. Also of interest, a rapid water loss event was witnessed for 0 POSS in the vicinity of its T_g marked by significant probe vibration (trace not shown). This event was not witnessed during the POSS-polyimide scans. This could be due to the lesser amounts of absorbed water in those materials or release during the scan prior to their T_gs because their densities are lower and diffusion coefficients are higher. Because of the speed of the scan, the former is more likely, but the latter possibility cannot be ignored.

Thermal Stability. The thermal stabilities of the polyimides were investigated by TGA in both inert (N_2) and oxidizing (air) atmospheres at a scan rate of 10 °C min^{-1}. One hour isothermal steps at 370 °C were instituted to determine mass losses during cure. The data are plotted in Figure 14 (a) N_2 and (b) air, and

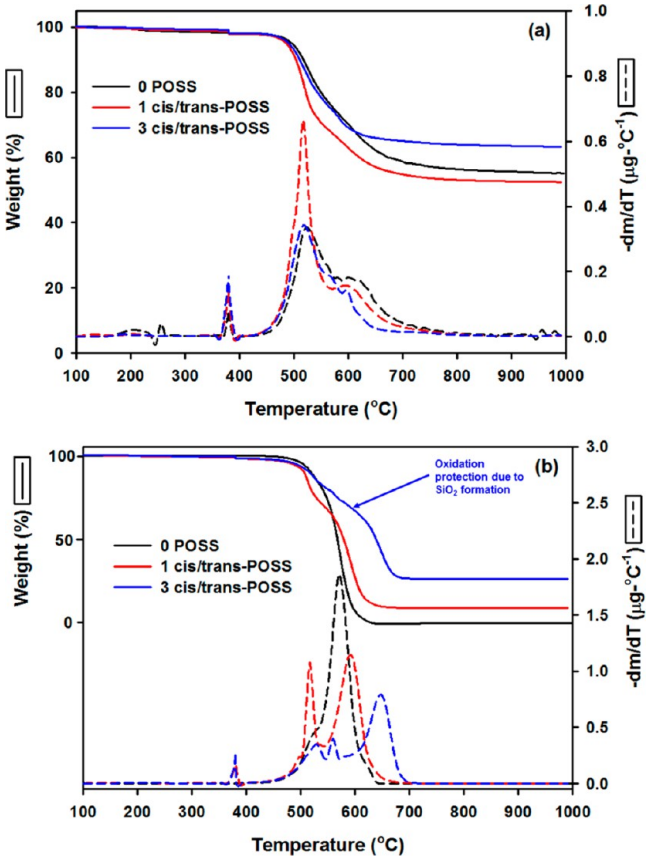

Figure 14. Mass loss profiles [solid lines] and their first derivatives (where m = mass) [dashed lines] for all oligomers, in (a) N_2 and (b) air, at a scan rate of 10 °C min^{-1}. Improved thermo-oxidative stability for the 3 POSS polyimides is highlighted in (b).

both the mass loss profiles and their first derivatives with respect to temperature are depicted. For clarity, only data pertaining to the 0 POSS and cis/trans oligomers are shown, since isomer type was found to exert marginal effects on mass loss characteristics. Examining the mass loss profiles, limited mass, attributed to trapped NMP solvent from synthesis, is lost in the vicinity of 150 °C. Additional mass is lost for many of the oligomers during the isothermal event, which may be attributed to unreacted monomers or dimers. The principal mass loss statistics for all of the oligomers are also shown in Table 7. In an N_2 atmosphere, two mechanistic degradation steps are witnessed, with the first, more significant event, commencing at ~415 °C. The thermal stabilities of the POSS polyimides are slightly lower than 0 POSS as evidenced by in most cases a 10−15 °C reduction in the 5 and 10% loss temperatures ($T_{d,5}$ and $T_{d,10}$, respectively). The magnitudes of the first weight loss event are greater for the 1 POSS polyimides, but those of the 3 POSS are similar to 0 POSS. The second mass loss event is suppressed for the 3 POSS polyimides, leading to a higher char yield, as quantified in Table 7. This may be attributed to a higher concentration of phenyl

dx.doi.org/10.1021/ma401347q | Macromolecules 2013, 46, 7363−7377

Table 7. TGA Weight Loss Statistics Determined from the Data Presented in Figure 15

	N_2				air		
oligomer	$T_{d,5}$ (°C)	$T_{d,10}$ (°C)	char yield[a] (%)	char yield[b] (%)	$T_{d,5}$ (°C)	$T_{d,10}$ (°C)	char yield[a] (%)
0 POSS	508	523	57.2	0.0 (0.0)	499	516	0.0 (0.0)
1 cis/trans-POSS	499	513	54.6	7.7 (14.2)	497	511	10.6 (14.2)
1 cis-POSS	493	504	53.0	6.1 (14.2)	480	497	10.0 (14.2)
1 trans-POSS	494	507	47.8	7.3 (14.2)	490	506	11.6 (14.2)
3 cis/trans-POSS	499	516	65.1	–[c] (27.7)	502	522	28 (27.7)
3 cis-POSS	493	512	63.7	–[c] (27.7)	490	511	26.1 (27.7)
3 trans-POSS	493	512	65.3	30.3 (27.7)	493	516	28.6 (27.7)

[a]Char yield resulting after a 10 °C min^{-1} scan to 1000 °C in a chosen atmosphere. [b]Oxidized mass yield of char rendered from char yield in N_2. [c]Not measured.

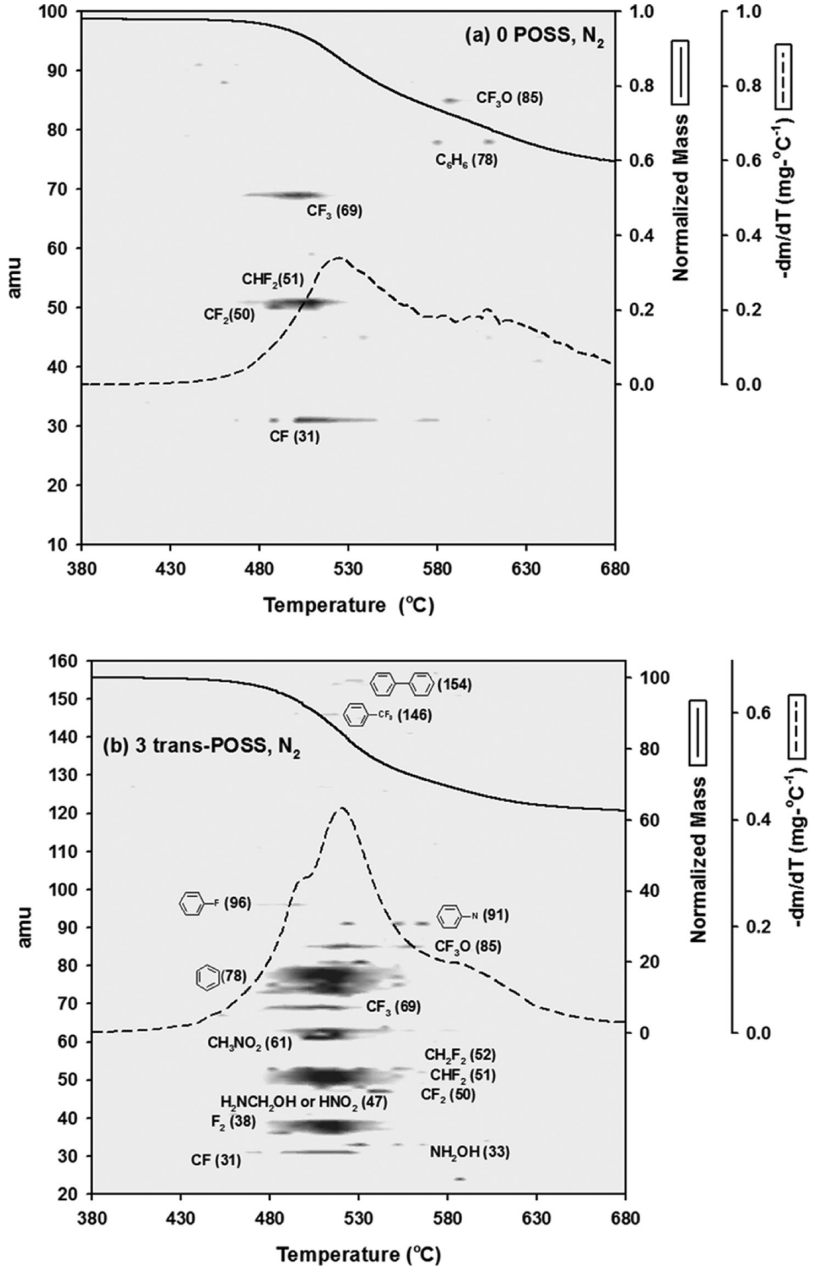

Figure 15. 2-D gray intensity contour plots of detected fragments during mass spectrometry of the pyrolysis products of (a) 0 POSS and (b) 3 trans-POSS, in a nitrogen atmosphere. The mass loss profiles (solid lines) and their first derivatives (dashed) are overlaid.

hydrogens which, upon cleavage during pyrolysis, form reactive intermediates that promote additional cross-linking.[39] The chars resulting from inert atmosphere pyrolysis were further heat treated in air to determine their SiO content. Comparison with

dx.doi.org/10.1021/ma401347q | Macromolecules 2013, 46, 7363–7377

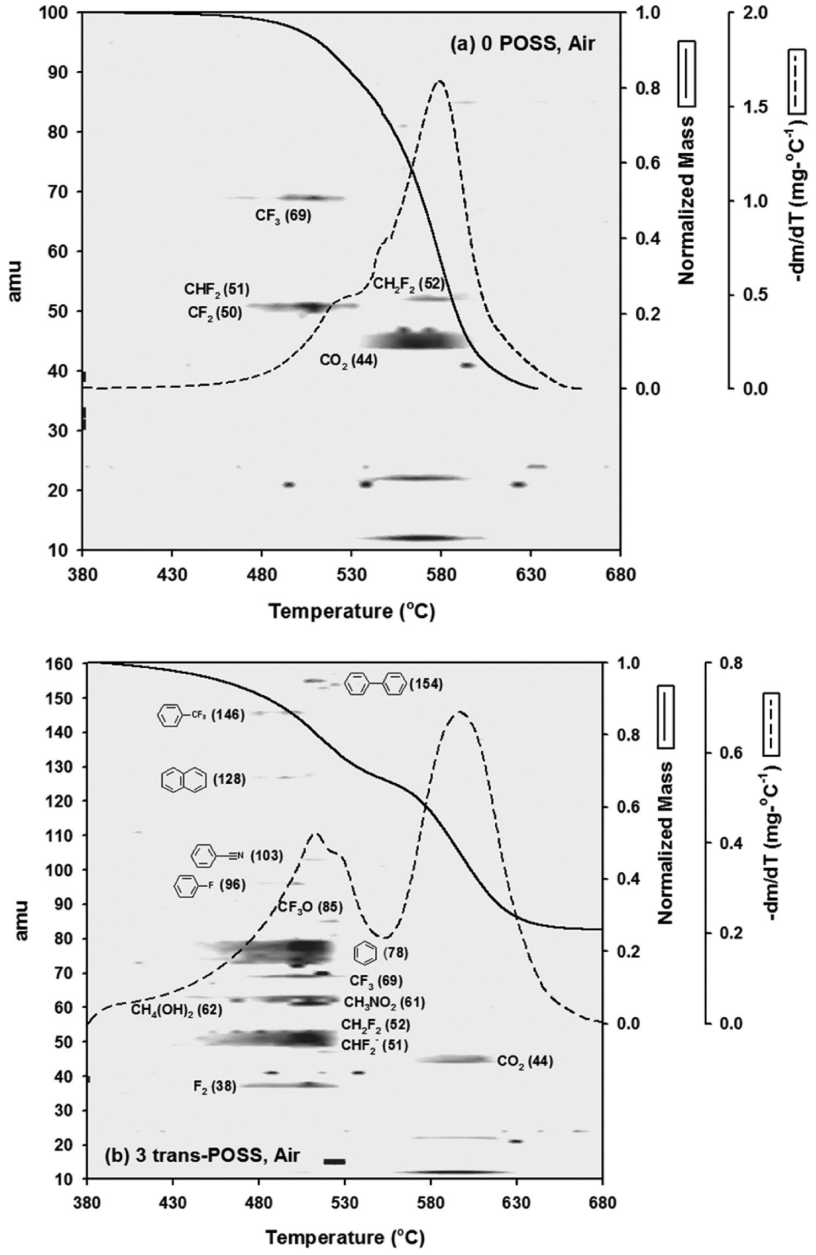

Figure 16. 2-D gray intensity contour plots of detected fragments during mass spectrometry of the pyrolysis products of (a) 0 POSS and (b) 3 trans-POSS, in air.

the theoretical yields of SiO_2 based on oligomeric $Si_{10}O_{14}$ content suggests that Si fragments are lost during one of the pyrolyzing exposures of the 1 POSS polyimides, but not for 3 POSS.

More appreciable differences in degradation behavior occur in air. Again, two primary events are apparent in the first-derivative profile for 0 POSS, but more complex behavior is witnessed for the POSS-containing oligomers. For 0 POSS, the two mass loss mechanisms are more convoluted than those seen in nitrogen, with the first being of lower intensity, opposite that in inert conditions. Expectedly, oxidative pyrolysis of 0 POSS produces no residual char mass. For 1 POSS, two distinct events are more apparent and are of approximately equivalent intensity. Most distinguishing, the 3 POSS polymers begin to lose mass at similar temperatures as those of 0 and 1 POSS, but mass loss is markedly suppressed in the early stages of decomposition. We attribute this behavior to POSS cage oxidation resulting in the formation of SiO_2 which provides protection to the remaining polymer. The most significant mass loss for the 3 POSS polyimides ccurs above 600 °C, due to the oxidation of the remaining polymer. Examining the weight loss statistics in Table 7, it is evident that the 5 and 10% weight loss temperatures ($T_{d,5}$ and $T_{d,10}$, respectively) for the 3 POSS polyimides are equivalent or superior to those of the other oligomer types, but these characteristics fail to capture the protective nature of POSS. In terms of char yield, which is expected to be pure SiO_2 in this environment, similar behavior is witnessed to that of the N_2 experiments in that the theoretical yield is produced for the 3 POSS polyimides but is less than expected for the 1 POSS materials, again suggesting that Si-containing fragments are lost in the latter.

Mass spectrometry was performed on the degradation products of the 0 POSS and 3 trans-POSS polyimides, in both inert and oxidizing atmospheres, in concert with TGA, to further

dx.doi.org/10.1021/ma401347q | *Macromolecules* 2013, 46, 7363−7377

our understanding of degradation mechanisms. The results are plotted in Figure 15 (N_2) and Figure 16 (air), in 2-D gray intensity contour format, illustrating amu fragment detection as a function of dynamic TGA temperature. We have attempted to identify the most prolifically detected fragments. Gray intensity is proportional to detected amu counts; corresponding TGA mass loss profiles and their first derivatives are overlaid. For 0 POSS, two events are found to occur during N_2 pyrolysis. In the first, commencing at 470 °C, CF_3 scission from the 6-FDA segment is witnessed (69 amu), and detection of CHF_2 (51), CF_2 (50), and CF (31) is also detected. In the second, less pronounced event initiating at 580 °C, the CF_3O^- anion (85) is detected as well as the products of weak polymer chain scission resulting in the release of benzene (78) and CO_2 (44). CF_3O^- emanates from reactions with CO and CO_2, which are conceived from fragmentation of anhydride groups. No nitrogen-containing species are detected, and the 0 POSS pyrolyzes to a high char yield at 1000 °C (0.57).

Pyrolysis of 3 trans-POSS is more complex and appears to transpire by three convoluted mechanisms. The first, commencing at ∼470 °C, again involves CF_3 scission from 6-FDA, but phenyl groups peripheral to POSS cleave simultaneously, primarily rendering benzene and its fragments (37−39, 50−52, 63, 73−79). Consistently, scission of phenyl groups covalently attached to POSS has been reported to occur at ∼480 °C.[40] Trace fluorobenzene (96) is also detected, resulting from a cross-reaction between the two primary products. The higher temperature steps appear to involve additional backbone scission, and several nitrogen-containing and aromatic fragments are detected, including hydroxylamine (33), methanol amine or nitrous acid (47), nitromethane (61), the CF_3O^- anion, and nitrobenzene (91) as well as minute detection of higher mass fragments 146 (trifluoromethylbenzene) and 154 (biphenyl). The greater number of nitrogen-containing fragments suggests a higher degree of backbone fragmentation relative to 0 POSS, although no POSS fragments are detected, and yet a higher char yield is produced (∼0.63).

Also shown in Figure 16, oxidative degradation of 0 POSS in air occurs in two primary steps, similar to nitrogen pyrolysis. CF_3 scission from 6-FDA is detected first, as well as its fluorinated byproducts, and in the second step, complete backbone oxidation occurs, primarily resulting in CO_2 (44, 22, 12). Oxidation of 3 trans-POSS also occurs in two primary steps, but the fragmentation pattern is much broader in terms of detected species. CF_3 scission occurs concurrently with POSS periphery detachment, rendering a number of species, including fluorine (38), CF_3, CF_3O^-, and benzene. Cross- and inter-reactions produce higher amu fragments including fluorobenzene, naphthalene, trifluoromethylbenzene, and biphenyl. We have also identified in the first step a degree of additional backbone oxidation, producing ethylene glycol (62) as well as a few nitrogen-containing species including nitromethane and benzonitrile (103). In the second step, all remaining organics are oxidized to CO_2, leaving a residue composed of the theoretical yield of SiO_2, based on POSS SiO content. No fluorinated species are detected during this step.

4. CONCLUSIONS

A POSS dianiline, possessing a thermally stable aromatic periphery, was co-oligomerized with 6-FDA, ODA, and PEPA end-cap to form thermosetting oligoimides with average repeat units of n = 4, in good yield. The POSS cage remained intact during synthesis. Because of regioisomerism, this POSS unit provided the ability to determine isomer-property effects, and we discovered that this isomerism impacts oligomer rheological characteristics and cure behavior, but little effect was observed on cured state properties. The benefits of POSS co-oligomerization are threefold: (1) in most cases, processing viscosity was reduced by nearly an order of magnitude, (2) overall thermal stability improved in both inert and oxidizing atmospheres, and (3) improved moisture resistance. All of these benefits are augmented with increased POSS content. Contrarily, at a fixed number of repeat units, POSS oligomerization was found to reduce cured T_g due to increased length and molecular weight between cross-link junctions. The selected POSS dianiline, due to its chemical architecture, provides a good choice for oligoimide modification because its thermal stability is similar to many monomers used in high performance thermosetting polyimides, with the added benefit of forming protective inorganic species during thermo-oxidative degradation. Based on these initial results, hybrid resin systems are expected to play an important role in next-generation thermoset materials due to their improved thermo-oxidative stability and enhanced hydrophobic character.

AUTHOR INFORMATION

Corresponding Author

*E-mail: gregory.yandek@edwards.af.mil (G.R.Y.).

Notes

The authors declare no competing financial interest.

ACKNOWLEDGMENTS

We gratefully thank the Air Force Office of Scientific Research as well as the Rocket Propulsion Division of AFRL's Aerospace Systems Directorate for financial support.

REFERENCES

(1) Michandani, G.; Shertukde, V. *Pop. Plast. Packag.* **2004**, *49* (7), 63−73.
(2) Meador, M. A. *Annu. Rev. Mater. Res.* **1998**, *28*, 599.
(3) Harvey, J. A. *Process., Fabr. Appl. Adv. Compos., Proc. Conf.* **1993**, 199−202.
(4) Scola, D. A. *Polyimides Other High-Temp. Polym., Proc. Eur. Tech. Symp., 2nd* **1991**, 265−81.
(5) Tang, H.; Feng, H.; Luo, H.; Dong, L.; Feng, Z. *Eur. Polym. J.* **1997**, *33* (4), 519−23.
(6) Hasegawa, M.; Ishii, J.; Matano, T.; Shindo, Y.; Sugimura, T.; Miwa, T.; Ishida, M.; Okabe, Y.; Takahashi, A. *ACS Symp. Ser.* **1995**, *614* (Microelectronics Technology), 395−412.
(7) Mensitieri, G.; Lavorgna, M.; Larobina, D.; Scherillo, G.; Ragosta, G.; Musto, P. *Macromolecules* **2008**, *41*, 4850−55.
(8) Pranjoto, H.; Denton, D. *J. Appl. Polym. Sci.* **1991**, *42* (1), 75−83.
(9) Lee, C.; Shul, Y.; Han, H. *J. Polym. Sci., Part B: Polym. Phys.* **2002**, *40*, 2190−98.
(10) Cauch-Cupul, J. I.; Perez-Pacheco, E.; Valadez-Gonzalez, A.; Herrera-Franco, P. J. *J. Mater. Sci.* **2011**, *46*, 6664−72.
(11) Bao, L.-R.; Yee, A. F. *Compos. Sci. Technol.* **2002**, *62*, 2099−2110.
(12) Lv, X.; Wang, R.; Liu, W.; Jiang, L. *Appl. Surf. Sci.* **2011**, *257*, 10459−64.
(13) Czabaj, M. W.; Zehnder, A. T.; Hui, C.-Y. *Composites, Part B* **2010**, *41*, 568−77.
(14) Wang, H.-W.; Dong, R.-X.; Liu, C.-L.; Chang, H.-Y. *J. Appl. Polym. Sci.* **2007**, *104* (1), 318−24.
(15) Leu, C.-M.; Wu, Z.-W.; Wei, K.-H. *Chem. Mater.* **2002**, *14* (7), 3016−3021.
(16) Tyan, H.-L.; Wu, C.-Y.; Wei, K.-H. *J. Appl. Polym. Sci.* **2001**, *81* (7), 1742−47.

(17) Banerjee, S.; Madhra, M. K.; Salunke, A. K.; Jaiswal, D. K. *Polymer* **2002**, *44* (3), 613−622.
(18) Wang, C.-Y.; Li, G.; Zhao, X.-Y.; Jiang, J.-M. *J. Polym. Sci., Part A: Polym. Chem.* **2009**, *47* (13), 3309−17.
(19) Chern, Y.-T.; Tsai, J.-Y. *Macromolecules* **2008**, *21* (24), 9556−9564.
(20) Biolley, N.; Gregoire, M.; Pascal, T.; Sillion, B. *Polymer* **1991**, *32* (17), 3256−61.
(21) Policastro, P. P.; Lupinski, J. H.; Hernandez, P. K. *Polym. Mater. Sci. Eng.* **1988**, *59*, 209−13.
(22) Arnold, C. A.; Summers, J. D.; Chen, Y. P.; Bott, R. H.; Chen, D.; McGrath, J. E. *Polymer* **1989**, *30* (6), 986−95.
(23) Wu, S.; Hayakawa, T.; Kikuchi, R.; Grunzinger, S. J.; Kakimoto, M.-A.; Oikawa, H. *Macromolecules* **2007**, *40* (16), 5698−5705.
(24) Wright, M. E.; Schorzman, D. A.; Feher, F. J.; Jin, R.-Z. *Chem. Mater.* **2003**, *15*, 264−68.
(25) Seurer, B.; Haddad, T.; Mabry, J. M.; Lee, A. *Macromolecules* **2010**, *43*, 9337−47.
(26) Vij, V.; Yandek, G.; Ramirez, S.; Mabry, J.; Haddad, T. *Silicon* **2012**, *4*, 267−80.
(27) Pascault, J. P.; Williams, R. J. J. *J. Polym. Sci., Part B: Polym. Phys.* **1990**, *28*, 85.
(28) DiBenedetto, A. T. *J. Polym. Sci., Part B: Polym. Phys.* **1987**, *25*, 1949.
(29) Fang, X.; Rogers, D. F.; Scola, D. A.; Stevens, M. P. *J. Polym. Sci., Part A: Polym. Chem.* **1998**, *36*, 461−70.
(30) Li, Y.; Morgan, R. J. *J. Appl. Polym. Sci.* **2006**, *101*, 4446−53.
(31) Wright, M. E.; Petteys, B. J.; Guenthner, A. J.; Fallis, S.; Yandek, G. R.; Tomczak, S. J.; Minton, T. K.; Brunsvold, A. *Macromolecules* **2006**, *39*, 4710−18.
(32) Wright, M. E.; Schorzman, D. A. *Macromolecules* **1999**, *32*, 8693−94.
(33) Vijayaraghavan, R.; Scola, D. A.; Sung, C. S. P. *Composites, Part A* **2009**, *40*, 2054−63.
(34) Russell, J. D.; Kardos, J. L. *Polym. Compos.* **1997**, *18*, 64.
(35) Lu, M. G.; Shim, M. J.; Kim, S. W. *J. Therm. Anal. Calorim.* **1999**, *58*, 701−9.
(36) Xu, W. B.; Zhou, Z. F.; He, P. S.; Pan, W.-P. *J. Therm. Anal. Calorim.* **2004**, *78*, 113−24.
(37) Takekoshi, T.; Terry, J. M. *Polymer* **1994**, *35*, 4874−80.
(38) Lee, C.; Shul, Y.; Han, H. *J. Polym. Sci., Part B: Polym. Phys.* **2002**, *40*, 2190−98.
(39) Xie, W.; Pan, W.-P.; Chuang, K. C. *Thermochim. Acta* **2001**, *367*−*368*, 143−53.
(40) Yandek, G. R.; Moore, B. M.; Ramirez, S. M.; Mabry, J. M. *J. Phys. Chem. C* **2012**, *116*, 16755−65.